

# Fundamental limits on the rate of bacterial cell division

**Nathan M. Belliveau<sup>†, 1</sup>, Griffin Chure<sup>†, 2, 3</sup>, Christina L. Hueschen<sup>4</sup>, Hernan G. Garcia<sup>5</sup>, Jané Kondev<sup>6</sup>, Daniel S. Fisher<sup>7</sup>, Julie Theriot<sup>1, 8</sup>, Rob Phillips<sup>2, 9,\*</sup>**

\*For correspondence:

<sup>†</sup>These authors contributed equally to this work

<sup>1</sup>Department of Biology, University of Washington, Seattle, WA, USA; <sup>2</sup>Division of Biology and Biological Engineering, California Institute of Technology, Pasadena, CA, USA; <sup>3</sup>Department of Applied Physics, California Institute of Technology, Pasadena, CA, USA; <sup>4</sup>Department of Chemical Engineering, Stanford University, Stanford, CA, USA; <sup>5</sup>Department of Molecular Cell Biology and Department of Physics, University of California Berkeley, Berkeley, CA, USA; <sup>6</sup>Department of Physics, Brandeis University, Waltham, MA, USA; <sup>7</sup>Department of Applied Physics, Stanford University, Stanford, CA, USA; <sup>8</sup>Allen Institute for Cell Science, Seattle, WA, USA; <sup>9</sup>Department of Physics, California Institute of Technology, Pasadena, CA, USA; \*Contributed equally

## Abstract

## Introduction

The range of bacterial growth rates is enormously diverse. In natural environments, some microbial organisms might double only once per year while in comfortable laboratory conditions, growth can be rapid with several divisions per hour. This six order of magnitude difference illustrates the intimate relationship between environmental conditions and the rates at which cells convert nutrients into new cellular material – a relationship that has remained a major topic of inquiry in bacterial physiology for over a century (*Jun et al., 2018*). As was noted by Jacques Monod, “the study of the growth of bacterial cultures does not constitute a specialized subject or branch of research, it is the basic method of Microbiology.” Those words ring as true today as they did when they were written 70 years ago. Indeed, the study of bacterial growth has undergone a molecular resurgence since many of the key questions addressed by the pioneering efforts in the middle of the last century can be revisited by examining them through the lens of the increasingly refined molecular census that is available for bacteria such as the microbial workhorse *Escherichia coli*. Several of the outstanding questions that can now be studied about bacterial growth include: what sets the fastest time scale that bacteria can divide, and how is growth rate tied to the quality of the carbon source. In this paper, we address these two questions from two distinct angles. First, as a result of an array of high-quality proteome-wide measurements of the *E. coli* proteome under a myriad of different growth conditions, we have a census that allows us to explore how the number of key molecular players change as a function of growth rate. This census provides a window onto whether the processes they mediate such as molecular transport into the cells and molecular synthesis within cells can run faster. Second, because of our understanding of the molecular pathways responsible for many of the steps in bacterial growth, we can also make order of magnitude estimates to infer the copy numbers that would be needed to achieve a given growth rate. In this paper, we pass back and forth between the analysis of a variety of different proteomic datasets and order-of-magnitude estimations to determine possible molecular bottlenecks that limit bacterial growth and to see how

42 the growth rate varies in different carbon sources.

43 Specifically, we leverage a combination of *E. coli* proteomic data sets collected over the past  
 44 decade using either mass spectrometry (*Schmidt et al., 2016; Peebo et al., 2015; Valgepea et al.,*  
 45 **2013**) or ribosomal profiling (*Li et al., 2014*) across 31 unique growth conditions. Broadly speaking,  
 46 we entertain several classes of hypotheses as are illustrated in **Figure 1**. First, we consider potential  
 47 limits on the transport of nutrients into the cell. We address this hypothesis by performing an  
 48 order-of-magnitude estimate for how many carbon, phosphorous, and sulfur atoms are needed to  
 49 facilitate this requirement given a 5000 second division time. As a second hypothesis, we consider  
 50 the possibility that there exists a fundamental limit on how quickly the cell can generate ATP. We  
 51 approach this hypothesis from two angles, considering how many ATP synthase complexes must  
 52 be needed to churn out enough ATP to power protein translation followed by an estimation of  
 53 how many electron transport complexes must be present to maintain the proton motive force.  
 54 A third class of estimates considers the need to maintain the size and shape of the cell through  
 55 the construction of new lipids for the cell membranes as well as the glycan polymers which make  
 56 up the rigid peptidoglycan. Our final class of hypotheses centers on the synthesis of a variety of  
 57 biomolecules. Our focus is primarily on the stages of the central dogma as we estimate the number  
 58 of protein complexes needed for DNA replication, transcription, and protein translation.

59 In broad terms, we find that the majority of these estimates are in close agreement with the  
 60 experimental observations, with protein copy numbers apparently well-tuned for the task of cell  
 61 doubling. This allows us to systematically scratch off the hypotheses diagrammed in **Figure 1** as  
 62 setting possible speed limits. Ultimately, we find that protein translation (particularly the generation  
 63 of new ribosomes) acts as 1) a rate limiting step for the *fastest* bacterial division, and 2) the major  
 64 determinant of bacterial growth across all nutrient conditions we have considered under steady  
 65 state, exponential growth. This perspective is in line with the linear correlation observed between  
 66 growth rate and ribosomal content (typically quantified through the ratio of RNA to protein) for fast  
 67 growing cells (*Scott et al., 2010*), but suggests a more prominent role for ribosomes in setting the  
 68 doubling time across all conditions of nutrient limitation. Here we again leverage the quantitative  
 69 nature of this data set and present a quantitative model of the relationship between the fraction of  
 70 the proteome devoted to ribosomes and the speed limit of translation, revealing a fundamental  
 71 tradeoff between the translation capacity of the ribosome pool and the maximal growth rate.

## 72 Uptake of Nutrients

73 In order to build new cellular mass, the molecular and elemental building blocks must be scavenged  
 74 from the environment in different forms. Carbon, for example, is acquired via the transport of  
 75 carbohydrates and sugar alcohols with some carbon sources receiving preferential treatment  
 76 in their consumption (*Monod, 1947*). Phosphorus, sulfur, and nitrogen, on the other hand, are  
 77 harvested primarily in the forms of inorganic salts, namely phosphate, sulfate, and ammonia  
 78 (*Jun et al., 2018; Assentoft et al., 2016; Stasi et al., 2019; Antonenko et al., 1997; Rosenberg et al.,*  
 79 **1977; Willsky et al., 1973**). All of these compounds have different permeabilities across the cell  
 80 membrane and most require some energetic investment either via ATP hydrolysis or through the  
 81 proton electrochemical gradient to bring the material across the hydrophobic cell membrane. Given  
 82 the diversity of biological transport mechanisms and the vast number of inputs needed to build a  
 83 cell, we begin by considering transport of some of the most important cellular ingredients: carbon,  
 84 nitrogen, oxygen, hydrogen, phosphorus, and sulfur.

85 The elemental composition of *E. coli* has received much quantitative attention over the past  
 86 half century (*Neidhardt et al., 1991; Taymaz-Nikerel et al., 2010; Heldal et al., 1985; Bauer and Ziv,*  
 87 **1976**), providing us with a starting point for estimating the copy numbers of various transporters.  
 88 While there is some variability in the exact elemental percentages (with different uncertainties), we  
 89 can estimate that the dry mass of a typical *E. coli* cell is  $\approx$  45% carbon (BNID: 100649, *Milo et al.*  
 90 **(2010)**),  $\approx$  15% nitrogen (BNID: 106666, *Milo et al. (2010)*),  $\approx$  3% phosphorus (BNID: 100653, *Milo*  
 91 **et al. (2010)**), and 1% sulfur (BNID: 100655, *Milo et al. (2010)*). In the coming paragraphs, we will

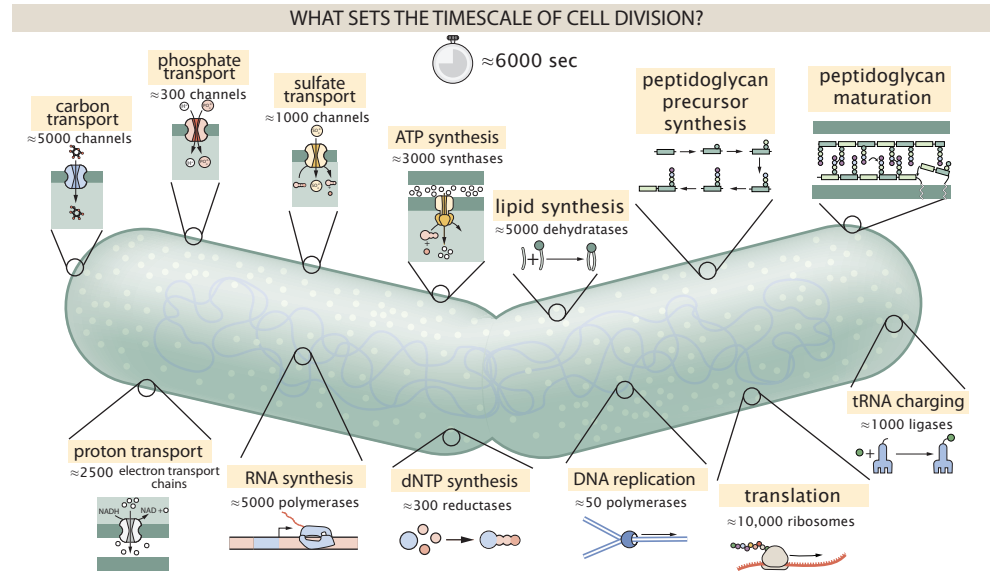


**Figure 1. Transport and synthesis processes necessary for cell division.** We consider an array of processes necessary for a cell to double its molecular components. Such processes include the transport of carbon across the cell membrane, the production of ATP, and fundamental processes of the central dogma namely RNA, DNA, and protein synthesis. A schematic of each synthetic or transport category is shown with an approximate measure of the complex abundance at a growth rate of 0.5 per hour. In this work, we consider a standard bacterial division time of  $\approx 5000$  sec.

92 engage in a dialogue between back-of-the-envelope estimates for the numbers of transporters  
 93 needed to facilitate these chemical stoichiometries and the experimental proteomic measurements  
 94 of the biological reality. Such an approach provides the opportunity to test if our biological knowl-  
 95 edge is sufficient to understand the scale at which these complexes are produced. Specifically, we  
 96 will make these estimates considering a modest doubling time of 5000 s, a growth rate of  $\approx 0.5 \text{ hr}^{-1}$ ,  
 97 the range in which the majority of the experimental measurements reside.

### 98 Carbon Transport

99 We begin with the most abundant element by mass, carbon. Using  $\approx 0.3 \text{ pg}$  as the typical *E. coli*  
 100 dry mass (BNID: 103904, *Milo et al. (2010)*), we estimate that  $\approx 10^{10}$  carbon atoms must be brought  
 101 into the cell in order to double all of the carbon-containing molecules (*Figure 2(A, top)*). Typical  
 102 laboratory growth conditions, such as those explored in the aforementioned proteomic data sets,  
 103 provide carbon as a single class of sugar such as glucose, galactose, or xylose to name a few. *E.*  
 104 *coli* has evolved myriad mechanisms by which these sugars can be transported across the cell  
 105 membrane. One such mechanism of transport is via the PTS system which is a highly modular  
 106 system capable of transporting a diverse range of sugars (*Escalante et al., 2012*). The glucose-  
 107 specific component of this system transports  $\approx 200$  glucose molecules per second per channel  
 108 (BNID: 114686, *Milo et al. (2010)*). Making the assumption that this is a typical sugar transport rate,  
 109 coupled with the need to transport  $10^{10}$  carbon atoms, we arrive at the conclusion that on the order  
 110 of 1,000 transporters must be expressed in order to bring in enough carbon atoms to divide in  
 111 6,000 s, diagrammed in the top panel of *Figure 2(A)*. This estimate, along with the observed average  
 112 number of carbohydrate transporters present in the proteomic data sets (*Schmidt et al., 2016*;  
 113 *Peebo et al., 2015; Valgepea et al., 2013; Li et al., 2014*), is shown in *Figure 2(A)*. While we estimate  
 114 1,000 transporters are needed, the data reveals that at a division time of  $\approx 5000$  s there is nearly  
 115 a ten-fold excess of transporters. Furthermore, the data illustrates that the average number of  
 116 carbohydrate transporters present is largely-growth rate independent.

117 The estimate presented in *Figure 2(A)* neglects any specifics of the regulation of carbon transport

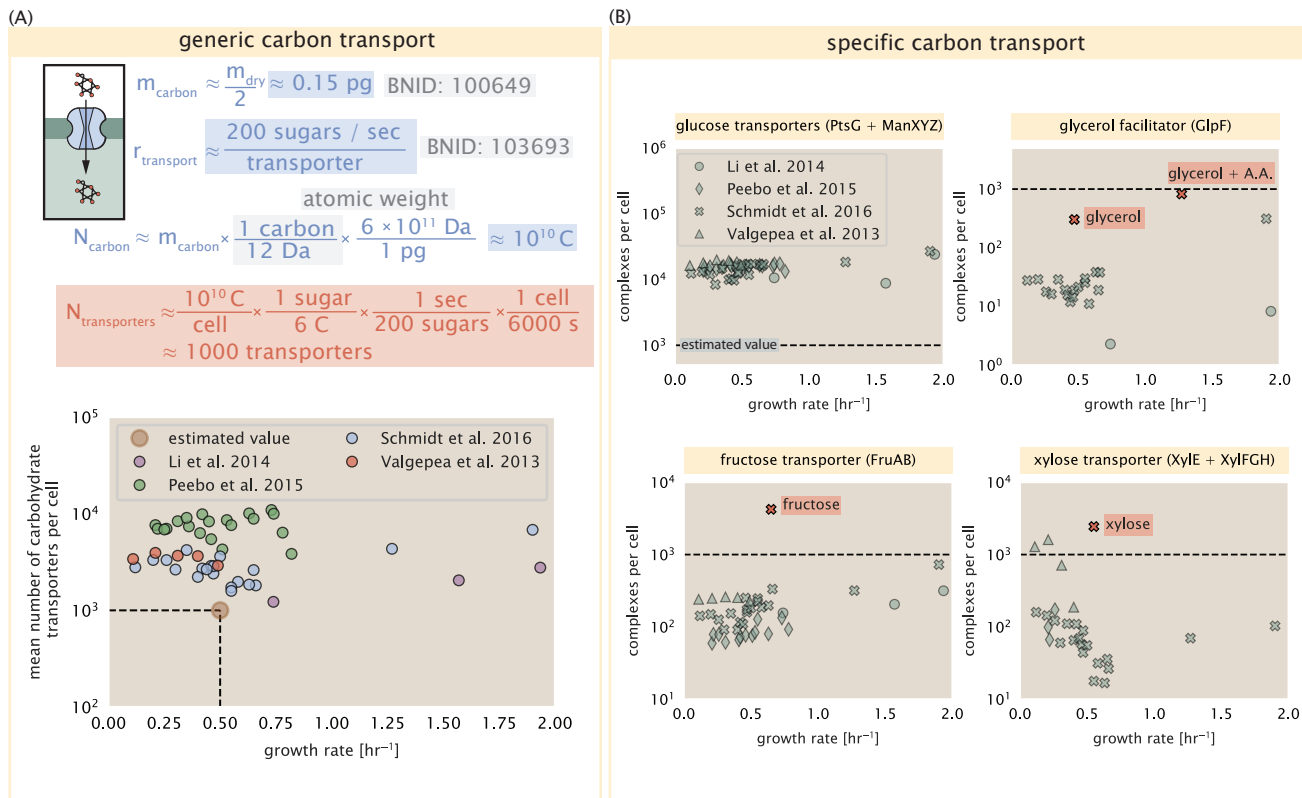


**Figure 2. The abundance of carbon transport systems across growth rates.** (A) A simple estimate for the minimum number of generic carbohydrate transport systems (top) assumes  $\approx 10^{10}$  C are needed to complete division, each transported sugar contains  $\approx 6$  C, and each transporter conducts sugar molecules at a rate of  $\approx 200$  per second. Bottom plot shows the estimated number of transporters needed at a growth rate of  $\approx 0.5$  per hr (light-brown point and dashed lines). Colored points correspond to the mean number of carbohydrate transporters for different growth conditions across different published datasets. (B) The abundance of various specific carbon transport systems plotted as a function of the population growth rate. Red points and red-highlighted text indicate conditions in which the only source of carbon in the growth medium induces expression of the transport system.

118 system and presents a data-averaged view of how many carbohydrate transporters are present  
 119 on average. Using the diverse array of growth conditions explored in the proteomic data sets, we  
 120 can explore how individual carbon transport systems depend on the population growth rate. In  
 121 **Figure 2(B)**, we show the total number of carbohydrate transporters specific to different carbon  
 122 sources. A striking observation, shown in the top-left plot of **Figure 2(B)**, is the constancy in the  
 123 expression of the glucose-specific transport systems (the PtsG enzyme of the PTS system and the  
 124 glucose-transporting ManXYZ complex). Additionally, we note that the total number of glucose-  
 125 specific transporters is tightly distributed  $\approx 10^4$  per cell, an order of magnitude beyond the estimate  
 126 shown in **Figure 2(A)**. This illustrates that *E. coli* maintains a substantial number of complexes  
 127 present for transporting glucose which is known to be the preferential carbon source (**Monod, 1947**;  
 128 **Liu et al., 2005; Aidelberg et al., 2014**).

129 It is now understood that a large number of metabolic operons are regulated with dual-input  
 130 logic gates that are only expressed when glucose concentrations are low (mediated by cyclic-AMP  
 131 receptor protein CRP) and the concentration of other carbon sources are elevated (**Gama-Castro**  
 132 **et al., 2016; Zhang et al., 2014b**). A famed example of such dual-input regulatory logic is in the  
 133 regulation of the *lac* operon which is only natively activated in the absence of glucose and the  
 134 presence of allolactose, an intermediate in lactose metabolism (**Jacob and Monod, 1961**), though we  
 135 now know of many other such examples (**Ireland et al., 2020; Gama-Castro et al., 2016; Belliveau**  
 136 **et al., 2018**). This illustrates that once glucose is depleted from the environment, cells have a means  
 137 to dramatically increase the abundance of the specific transporter needed to digest the next sugar  
 138 that is present. Several examples of induced expression of specific carbon-source transporters  
 139 are shown in **Figure 2(B)**. Points colored in red (labeled by red text-boxes) correspond to growth  
 140 conditions in which the specific carbon source (glycerol, xylose, or fructose) is present. These  
 141 plots show that, in the absence of the particular carbon source, expression of the transporters is  
 142 maintained on the order of  $\sim 10^2$  per cell. However, when induced, the transporters become highly-  
 143 expressed and are present on the order of  $\sim 10^4$  per cell, which exceeds the generic estimate given  
 144 in **Figure 2(A)**. Together, this generic estimation and the specific examples of induced expression  
 145 suggest that transport of carbon across the cell membrane, while critical for growth, is not the  
 146 rate-limiting step of cell division.

147 In the context of speeding up growth, one additional limitation is the fact that the cell's inner  
 148 membrane is occupied by a multitude of other membrane proteins. Considering a rule-of-thumb  
 149 for the surface area of *E. coli* of about  $6 \mu\text{m}^2$  (BNID: 101792, **Milo et al. (2010)**), we expect an  
 150 areal density for 1,000 transporters to be approximately 200 transporters/ $\mu\text{m}^2$ . For a glucose  
 151 transporter occupying about  $50 \text{ nm}^2/\text{dimer}$ , this amounts to about only 1 percent of the total inner  
 152 membrane (**Szenk et al., 2017**). In addition, bacterial cell membranes typically have densities of  
 153  $10^5$  proteins/ $\mu\text{m}^2$  (**Phillips, 2018**), implying that the cell could accommodate more transporters if it  
 154 were rate limiting.

### 155 Phosphorus and Sulfur Transport

156 We now turn our attention towards other essential elements, namely phosphorus and sulfur.  
 157 Phosphorus is critical to the cellular energy economy in the form of high-energy phosphodiester  
 158 bonds making up DNA, RNA, and the NTP energy pool as well as playing a critical role in the post-  
 159 translational modification of proteins and defining the polar-heads of lipids. In total, phosphorus  
 160 makes up  $\approx 3\%$  of the cellular dry mass which in typical experimental conditions is in the form of  
 161 inorganic phosphate. The cell membrane has remarkably low permeability to this highly-charged  
 162 and critical molecule, therefore requiring the expression of active transport systems. In *E. coli*, the  
 163 proton electrochemical gradient across the inner membrane is leveraged to transport inorganic  
 164 phosphate into the cell (**Rosenberg et al., 1977**). Proton-solute symporters are widespread in *E. coli*  
 165 (**Ramos and Kaback, 1977; Booth et al., 1979**) and can have rapid transport rates of 50 molecules  
 166 per second for sugars and other solutes (BNID: 103159; 111777, **Milo et al. (2010)**). In *E. coli* the PitA  
 167 phosphate transport system has been shown to very tightly coupled with the proton electrochemical

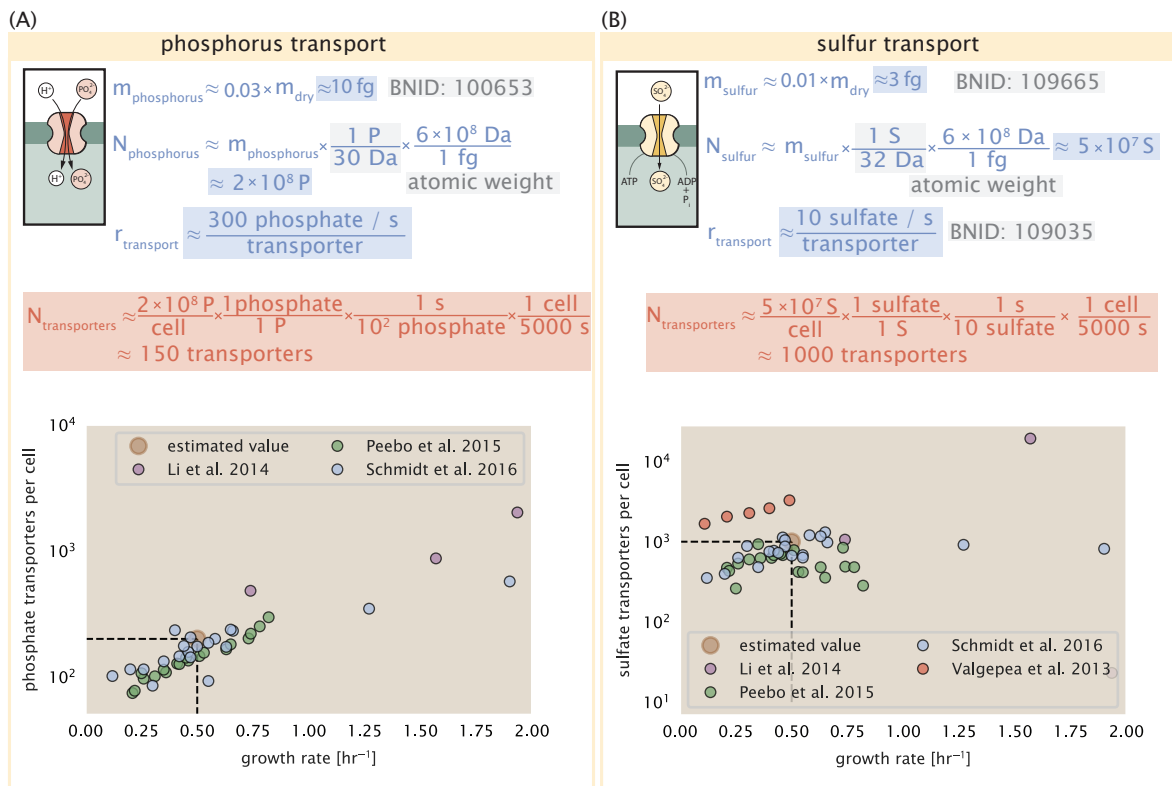


**Figure 3. Estimates and measurements of phosphate and sulfate transport systems as a function of growth rate.** (A) Estimate for the number of PitA phosphate transport systems needed to maintain a 3% phosphorus *E. coli* dry mass. Points in plot correspond to the total number of PitA transporters per cell. (B) Estimate of the number of CysUWA complexes necessary to maintain a 1% sulfur *E. coli* dry mass. Points in plot correspond to average number of CysUWA transporter complexes that can be formed given the transporter stoichiometry [CysA]<sub>2</sub>[CysU][CysW][Sbp/CysP].

gradient with a 1:1 proton:phosphate stoichiometric ratio (*Harris et al., 2001; Feist et al., 2007*). Illustrated in *Figure 3(A)*, we can estimate that  $\approx 300$  phosphate transporters are necessary to maintain an  $\approx 3\%$  dry mass with a 6,000 s division time. This estimate is again satisfied when we examine the observed copy numbers of PitA in proteomic data sets (plot in *Figure 3(A)*). While our estimate is very much in line with the observed numbers, we emphasize that this is likely a slight overestimate of the number of transporters needed as there are other phosphorous scavenging systems, such as the ATP-dependent phosphate transporter Pst system which we have neglected.

Satisfied that there are a sufficient number of phosphate transporters present in the cell, we now turn to sulfur transport as another potentially rate limiting process. Similar to phosphate, sulfate is highly-charged and not particularly membrane permeable, requiring active transport. While there exists a H<sup>+</sup>/sulfate symporter in *E. coli*, it is in relatively low abundance and is not well characterized (*Zhang et al., 2014a*). Sulfate is predominantly acquired via the ATP-dependent ABC transporter CysUWA system which also plays an important role in selenium transport (*Sekowska et al., 2000; Sirko et al., 1995*). While specific kinetic details of this transport system are not readily available, generic ATP transport systems in prokaryotes transport on the order of 1 to 10 molecules per second (BNID: 109035, *Milo et al. (2010)*). Combining this generic transport rate, measurement of sulfur comprising 1% of dry mass, and a 6,000 second division time yields an estimate of  $\approx 1000$  CysUWA complexes per cell (*Figure 3(B)*). Once again, this estimate is in notable agreement with proteomic data sets, suggesting that there are sufficient transporters present to acquire the necessary sulfur. In a similar spirit of our estimate of phosphorus transport, we emphasize that this is likely an overestimate of the number of necessary transporters as we have neglected other sulfur scavenging systems that are in lower abundance.

190 **Nitrogen Transport**

191 Finally, we turn to nitrogen transport as the last remaining transport system highlighted in **Figure 1**.  
 192 Unlike phosphate, sulfate, and various sugar molecules, nitrogen in the form of ammonia can readily  
 193 diffuse across the cell membrane and has a permeability on par with water ( $\approx 10^5$  nm/s, BNID:110824  
 194 *Milo et al. (2010)*). In particularly nitrogen-poor conditions, *E. coli* expresses a transporter (AmtB)  
 195 which appears to aid in nitrogen assimilation, though the mechanism and kinetic details of transport  
 196 is still a matter of debate (*van Heeswijk et al., 2013; Khademi et al., 2004*). Beyond ammonia,  
 197 another plentiful source of nitrogen come in the form of glutamate, which has its own complex  
 198 metabolism and scavenging pathways. However, nitrogen is plentiful in the growth conditions  
 199 examined in this work, permitting us to neglect nitrogen transport as a potential rate limiting  
 200 process in cell division.

201 **Function of the Central Dogma**

202 Up to this point, we have considered a variety of transport and biosynthetic processes that are  
 203 critical to acquiring and generating new cell mass. While there are of course many other metabolic  
 204 processes we could consider and perform estimates of (such as the components of fermentative  
 205 versus aerobic respiration), we now turn our focus to some of the most central processes which  
 206 must be undertaken irrespective of the growth conditions – the processes of the central dogma.

207 **DNA**

208 Most bacteria (including *E. coli*) harbor a single, circular chromosome and can have extra-chromosomal  
 209 plasmids up to  $\sim 100$  kbp in length. We will focus our quantitative thinking solely on the chromo-  
 210 some of *E. coli* which harbors  $\approx 5000$  genes and  $\approx 5 \times 10^6$  base pairs. To successfully divide and  
 211 produce viable progeny, this chromosome must be faithfully replicated and segregated into each  
 212 nascent cell. We again rely on the near century of literature in molecular biology to provide some  
 213 insight on the rates and mechanics of the replicative feat as well as the production of the required  
 214 starting materials, dNTPs.

215 **dNTP synthesis**

216 We begin our exploration DNA replication by examining the production of the deoxyribonucleotide  
 217 triphosphates (dNTPs). The four major dNTPs (dATP, dTTP, dCTP, and dGTP) are synthesized *de novo*  
 218 in separate pathways, requiring different building blocks. However, a critical step present in all  
 219 dNTP synthesis pathways is the conversion from ribonucleotide to deoxyribonucleotide via the  
 220 removal of the 3' hydroxyl group of the ribose ring (*Rudd et al., 2016*). This reaction is mediated by a  
 221 class of enzymes termed ribonucleotide reductases, of which *E. coli* possesses two aerobically active  
 222 complexes (termed I and II) and a single anaerobically active enzyme. Due to their peculiar formation  
 223 of a radical intermediate, these enzymes have received much biochemical, kinetic, and structural  
 224 characterization. One such work (*Ge et al., 2003*) performed a detailed *in vitro* measurement of the  
 225 steady-state kinetic rates of these complexes, revealing a turnover rate of  $\approx 10$  dNTP per second.

226 Since this reaction is central to the synthesis of all dNTPs, it is reasonable to consider the  
 227 abundance of these complexes is a measure of the total dNTP production in *E. coli*. Illustrated  
 228 schematically in **Figure 4** (A), we consider the fact that to replicate the cell's genome, on the order of  
 229  $\approx 10^7$  dNTPs must be synthesized. Assuming a production rate of 10 per second per ribonucleotide  
 230 reductase complex and a cell division time of 6000 seconds, we arrive at an estimate of  $\approx 150$   
 231 complexes needed per cell. As shown in the bottom panel of **Figure 4** (A), this estimate agrees  
 232 with the experimental measurements of these complexes abundances within  $\approx 1/2$  an order of  
 233 magnitude.

234 Recent work has revealed that during replication, the ribonucleotide reductase complexes  
 235 coalesce to form discrete foci colocalized with the DNA replisome complex (*Sánchez-Romero et al.,*  
 236 *2011*). This is particularly pronounced in conditions where growth is slow, indicating that spatial  
 237 organization and regulation of the activity of the complexes plays an important role.

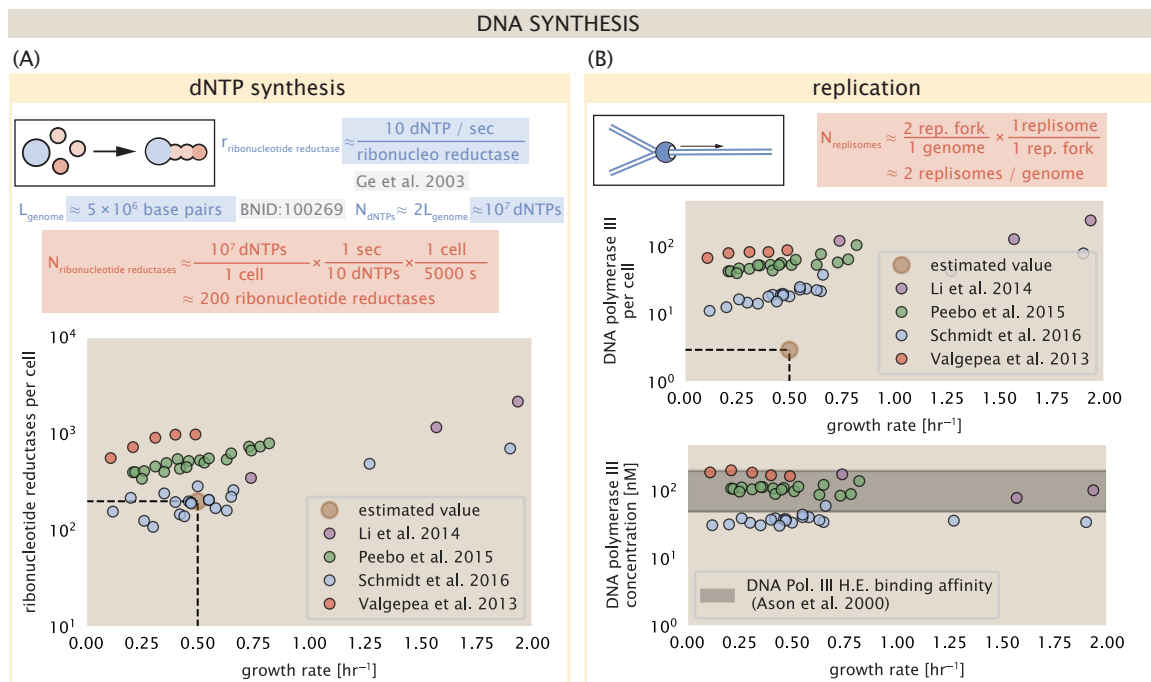


**Figure 4. Complex abundance estimates for dNTP synthesis and DNA replication.** (A) Estimate of the number of ribonucleotide reductase enzymes needed to facilitate the synthesis of  $\approx 10^7$  dNTPs over the course of a 6000 second generation time. Points in the plot correspond to the total number of ribonucleotide reductase I ( $[NrdA]_2[NrdB]_2$ ) and ribonucleotide reductase II ( $[NrdE]_2[NrdF]_2$ ) complexes. (B) An estimate for the minimum number of DNA polymerase holoenzyme complexes needed to facilitate replication of a single genome. Points in the top plot correspond to the total number of DNA polymerase III holoenzyme complexes ( $[DnaE]_3[DnaQ]_3[HolE]_3[DnaX]_5[HolB][HolA][DnaN]_4[HolC]_4[HolD]_4$ ) per cell. Bottom plot shows the effective concentration of DNA polymerase III holoenzyme given cell volumes calculated from the growth rate as in *Si et al. (2019)* (See Appendix Section 4).

## 238 DNA Replication

239 We now turn our focus to the integration of these dNTP building blocks into the replicated chromo-  
 240 some strand via the DNA polymerase. Replication is initiated at a single region of the chromosome  
 241 termed the *oriC* locus at which a pair of DNA polymerases bind and begin their high-fidelity replica-  
 242 tion of the genome in opposite directions. Assuming equivalence between the two replication forks,  
 243 this means that the two DNA polymerase complexes (termed replisomes) meet at the midway point  
 244 of the circular chromosome termed the *ter* locus. The kinetics of the five types of DNA polymerases  
 245 (I – V) have been intensely studied, revealing that DNA polymerase III performs the high fidelity  
 246 processive replication of the genome with the other "accessory" polymerases playing auxiliary roles  
 247 (*Fijalkowska et al., 2012*). *In vitro* measurements have shown that DNA Polymerase III copies DNA  
 248 at a rate of  $\approx$  600 nucleotides per second (BNID: 104120, *Milo et al. (2010)*). Therefore, to replicate a  
 249 single chromosome, two DNA polymerases replicating at their maximal rate would copy their entire  
 250 genome in  $\approx$  4000 s. Thus, with a division time of 5000 s (our "typical" growth rate for the purposes  
 251 of this work), there is sufficient time for a pair of DNA polymerase III complexes to replicate the  
 252 entire genome. However, this estimate implies that 4000 s would be the upper-limit time scale for  
 253 bacterial division which is at odds with the familiar 20 minute (1200 s) doubling time of *E. coli* in rich  
 254 medium.

255 It is well known that *E. coli* can parallelize its DNA replication such that multiple chromosomes  
 256 are being replicated at once, with as many as 10 - 12 replication forks at a given time (*Bremer*  
*and Dennis, 2008; Si et al., 2017*). Thus, even in rapidly growing cultures, we expect only a few  
 257 polymerases ( $\approx$  10) are needed to replicate the chromosome per cell doubling. However, as shown  
 258 in **Figure 4(B)**, DNA polymerase III is nearly an order of magnitude more abundant. This  
 259 discrepancy can be understood by considering its binding constant to DNA. DNA polymerase III  
 260 is highly processive, facilitated by a strong affinity of the complex to the DNA. *In vitro* biochemical  
 261 characterization has quantified the  $K_D$  of DNA polymerase III holoenzyme to single-stranded and  
 262 double-stranded DNA to be 50 and 200 nM, respectively (*Ason et al., 2000*). The bottom plot in  
 263 **Figure 4** (B) shows that the concentration of the DNA polymerase III across all data sets and growth  
 264 conditions is within this range. Thus, while the copy number of the DNA polymerase III is in excess  
 265 of the strict number required to replicate the genome, its copy number appears to vary such that its  
 266 concentration is approximately equal to the dissociation constant to the DNA. While the processes  
 267 regulating the initiation of DNA replication are complex and involve more than just the holoenzyme,  
 268 these data indicate that the kinetics of replication rather than the explicit copy number of the DNA  
 269 polymerase III holoenzyme is the more relevant feature of DNA replication to consider. In light  
 270 of this, the data in **Figure 4(B)** suggests that for bacteria like *E. coli*, DNA replication does not represent a rate-limiting step in cell division. However, it is worth noting that for bacterium like *C. crescentus* whose chromosomal replication is initiated only once per cell cycle (*Jensen et al., 2001*), the time to double their chromosome likely represents an upper limit to their growth rate.

## 275 RNA Synthesis

276 With the machinery governing the replication of the genome accounted for, we now turn our  
 277 attention to the next stage of the central dogma – the transcription of DNA to form RNA. We  
 278 primarily consider three major groupings of RNA, namely the RNA associated with ribosomes  
 279 (rRNA), the RNA encoding the amino-acid sequence of proteins (mRNA), and the RNA which links  
 280 codon sequence to amino-acid identity during translation (tRNA). Despite the varied function of  
 281 these RNA species, they share a commonality in that they are transcribed from DNA via the action  
 282 of RNA polymerase. In the coming paragraphs, we will consider the synthesis of RNA as a rate  
 283 limiting step in bacterial division by estimating how many RNA polymerases must be present to  
 284 synthesize all necessary rRNA, mRNA, and tRNA.

## 285 rRNA

286 We begin with an estimation of the number of RNA polymerases needed to synthesize the rRNA  
 287 that serve as catalytic and structural elements of the ribosome. Each ribosome contains three rRNA  
 288 molecules of lengths 120, 1542, and 2904 nucleotides (BNID: 108093, *Milo et al. (2010)*), meaning  
 289 each ribosome contains  $\approx$  4500 nucleotides. As the *E. coli* RNA polymerase transcribes DNA to RNA  
 290 at a rate of  $\approx$  40 nucleotides per second (BNID: 101904, *Milo et al. (2010)*), it takes a single RNA  
 291 polymerase  $\approx$  100 s to synthesize the RNA needed to form a single functional ribosome. Therefore,  
 292 in a 5000 s division time, a single RNA polymerase transcribing rRNA at a time would result in only  
 293  $\approx$  50 functional ribosomal rRNA units – far below the observed number of  $\approx$   $10^4$  ribosomes per cell.

294 Of course, there can be more than one RNA polymerase transcribing the rRNA genes at any  
 295 given time. To elucidate the *maximum* number of rRNA units that can be synthesized given a single  
 296 copy of each rRNA gene, we will consider a hypothesis in which the rRNA operon is completely tiled  
 297 with RNA polymerase. *In vivo* measurements of the kinetics of rRNA transcription have revealed that  
 298 RNA polymerases are loaded onto the promoter of an rRNA gene at a rate of  $\approx$  1 per second (BNID:  
 299 111997; 102362, *Milo et al. (2010)*). If RNA polymerases are being constantly loaded on to the rRNA  
 300 genes at this rate, then we can assume that  $\approx$  1 functional rRNA unit is synthesized per second.  
 301 With a 5000 second division time, this hypothesis leads to a maximal value of 5000 functional rRNA  
 302 units, still undershooting the observed number of  $10^4$  ribosomes per cell.

303 *E. coli* has evolved a clever mechanism to surpass this kinetic limit for the rate of rRNA production.  
 304 Rather than having only one copy of each rRNA gene, *E. coli* has seven copies of the operon  
 305 (BIND: 100352, *Milo et al. (2010)*) four of which are localized directly adjacent to the origin of  
 306 replication (*Birnbaum and Kaplan, 1971*). As fast growth also implies an increased gene dosage due  
 307 to parallelized chromosomal replication, the total number of rRNA genes can be on the order of  $\approx$   
 308 10 – 70 copies at moderate to fast growth rates (*Stevenson and Schmidt, 2004*). Using our standard  
 309 time scale of a 5000 second division time, we can make the lower-bound estimate that the typical  
 310 cell will have 7 copies of the rRNA operon. Synthesizing one functional rRNA unit per second per  
 311 rRNA operon, a total of  $4 \times 10^4$  rRNA units can be synthesized, comfortably above the observed  
 312 number of ribosomes per cell.

313 How many RNA polymerases are then needed to constantly transcribe 7 copies of the rRNA  
 314 genes? We approach this estimate by considering the maximum number of RNA polymerases tiled  
 315 along the rRNA genes with a loading rate of 1 per second and a transcription rate of 40 nucleotides  
 316 per second. Considering that a RNA polymerase has a physical footprint of approximately 40  
 317 nucleotides (BNID: 107873, *Milo et al. (2010)*), we can expect  $\approx$  1 RNA polymerase per 80 nucleotides.  
 318 With a total length of  $\approx$  4500 nucleotides per operon and 7 operons per cell, the maximum number  
 319 of RNA polymerases that can be transcribing rRNA at any given time is  $\approx$  400. As we will see in the  
 320 coming sections, the synthesis of rRNA is the dominant requirement of the RNA polymerase pool.

## 321 mRNA

322 To form a functional protein, all protein coding genes must first be transcribed from DNA to form  
 323 an mRNA molecule. While each protein requires an mRNA blueprint, many copies of the protein  
 324 can be synthesized from a single mRNA. Factors such as strength of the ribosomal binding site,  
 325 mRNA stability, and rare codon usage frequency dictate the number of proteins that can be made  
 326 from a single mRNA, with yields ranging from  $10^1$  to  $10^4$  (BNID: 104186; 100196; 106254, *Milo et al.*  
 327 (*2010*)). Computing the geometric mean of this range yields  $\approx$  1000 proteins synthesized per mRNA,  
 328 a value that agrees with experimental measurements of the number of proteins per cell ( $\approx 3 \times 10^6$ ,  
 329 BNID: 100088, *Milo et al. (2010)*) and total number of mRNA per cell ( $\approx 3 \times 10^3$ , BNID: 100064, *Milo*  
 330 *et al. (2010)*).

331 This estimation captures the *steady-state* mRNA copy number, meaning that at any given time,  
 332 there will exist approximately 3000 unique mRNA molecules. To determine the *total* number of  
 333 mRNA that need to be synthesized over the cell's lifetime, we must consider degradation of the  
 334 mRNA. In most bacteria, mRNAs are rather unstable with life times on the order of several minutes

(BNID: 104324; 106253; 111927; 111998, *Milo et al. (2010)*). For convenience, we assume that the typical mRNA in our cell of interest has a typical lifetime of  $\approx$  300 seconds. Using this value, we can determine the total mRNA production rate to maintain a steady-state copy number of 3000 mRNA per cell. While we direct the reader to the appendix for a more detailed discussion of mRNA transcriptional dynamics, we state here that the total mRNA production rate must be on the order of  $\approx$  15 mRNA per second. In *E. coli*, the average protein is  $\approx$  300 amino acids in length (BNID: 108986; *Milo et al. (2010)*), meaning that the corresponding mRNA is  $\approx$  900 nucleotides which we will further approximate as  $\approx$  1000 nucleotides to account for the non-protein coding regions on the 5' and 3' ends. This means that the cell must have enough RNA polymerase molecules about to sustain a transcription rate of  $\approx 1.5 \times 10^4$  nucleotides per second. Knowing that a single RNA polymerase polymerizes RNA at a clip of 40 nucleotides per second, we arrive at a comfortable estimate of  $\approx$  250 RNA polymerase complexes needed to satisfy the mRNA demands of the cell. It is worth noting that this number is approximately half of that required to synthesize enough rRNA, as we saw in the previous section. We find this to be a striking result as these 250 RNA polymerase molecules are responsible for the transcription of the  $\approx$  4000 protein coding genes that are not ribosome associated.

### 351 tRNA

352 The final class of RNA molecules worthy of quantitative consideration is the pool of tRNAs used during translation to map codon sequence to amino acid identity. Unlike mRNA or rRNA, each individual tRNA is remarkably short, ranging from 70 to 95 nucleotides each (BNID: 109645; 353 102340, *Milo et al. (2010)*). What they lack in length, they make up for in abundance. There are 354 approximately  $\approx$  3000 tRNA molecules present for each of the 20 amino acids (BNID: 105280, *Milo et al. (2010)*), although the precise copy number is dependent on the identity of the ligated amino acid. Using these values, we make the estimate that  $\approx 5 \times 10^6$  nucleotides are sequestered in tRNA 355 per cell. Unlike mRNA, tRNA is remarkably stable with typical lifetimes *in vivo* on the order of  $\approx$  48 356 hours (*Abelson et al., 1974; Svenningsen et al., 2017*) – well beyond the timescale of division. Once 357 again using our rule-of-thumb for the rate of transcription to be 40 nucleotides per second and 358 assuming a division time of  $\approx$  5000 seconds, we arrive at an estimate of  $\approx$  20 RNA polymerases 359 to synthesize enough tRNA. This requirement pales in comparison to the number of polymerases 360 needed to generate the rRNA and mRNA pools and can be neglected as a significant transcriptional 361 burden.

### 366 RNA Polymerase and $\sigma$ -factor Abundance

367 These estimates, summarized in *Figure 5 (A)*, reveal that synthesis of rRNA and mRNA are the dominant 368 RNA species synthesized by RNA polymerase, suggesting the need for  $\approx$  700 RNA polymerases 369 per cell. As is revealed in *Figure 5 (B)*, this estimate is about an order of magnitude below the observed 370 number of RNA polymerase complexes per cell ( $\approx$  5000 - 7000). The disagreement between the estimated 371 number of RNA polymerases and these observations are at least consistent with recent literature 372 revealing that  $\approx$  80 % of RNA polymerases in *E. coli* are not transcriptionally active 373 (*Patrick et al., 2015*). Our estimate ignores the possibility that some fraction is only nonspecifically 374 bound to DNA, as well as the obstacles that RNA polymerase and DNA polymerase present for each 375 other as they move along the DNA (*Finkelstein and Greene, 2013*).

376 In addition, it is also vital to consider the role of  $\sigma$ -factors which help RNA polymerase identify 377 and bind to transcriptional start sites (*Browning and Busby, 2016*). Here we consider  $\sigma^{70}$  (RpoD) 378 which is the dominant "general-purpose"  $\sigma$ -factor in *E. coli*. While initially thought of as being solely 379 involved in transcriptional initiation, the past two decades of single-molecule work has revealed 380 a more multipurpose role for  $\sigma^{70}$  including facilitating transcriptional elongation (*Kapanidis et al., 2005; Goldman et al., 2015; Perdue and Roberts, 2011; Mooney and Landick, 2003; Mooney et al., 2005*). *Figure 5 (B)* is suggestive of such a role as the number of  $\sigma^{70}$  proteins per cell is in close 381 agreement with our estimate of the number of transcriptional complexes needed.

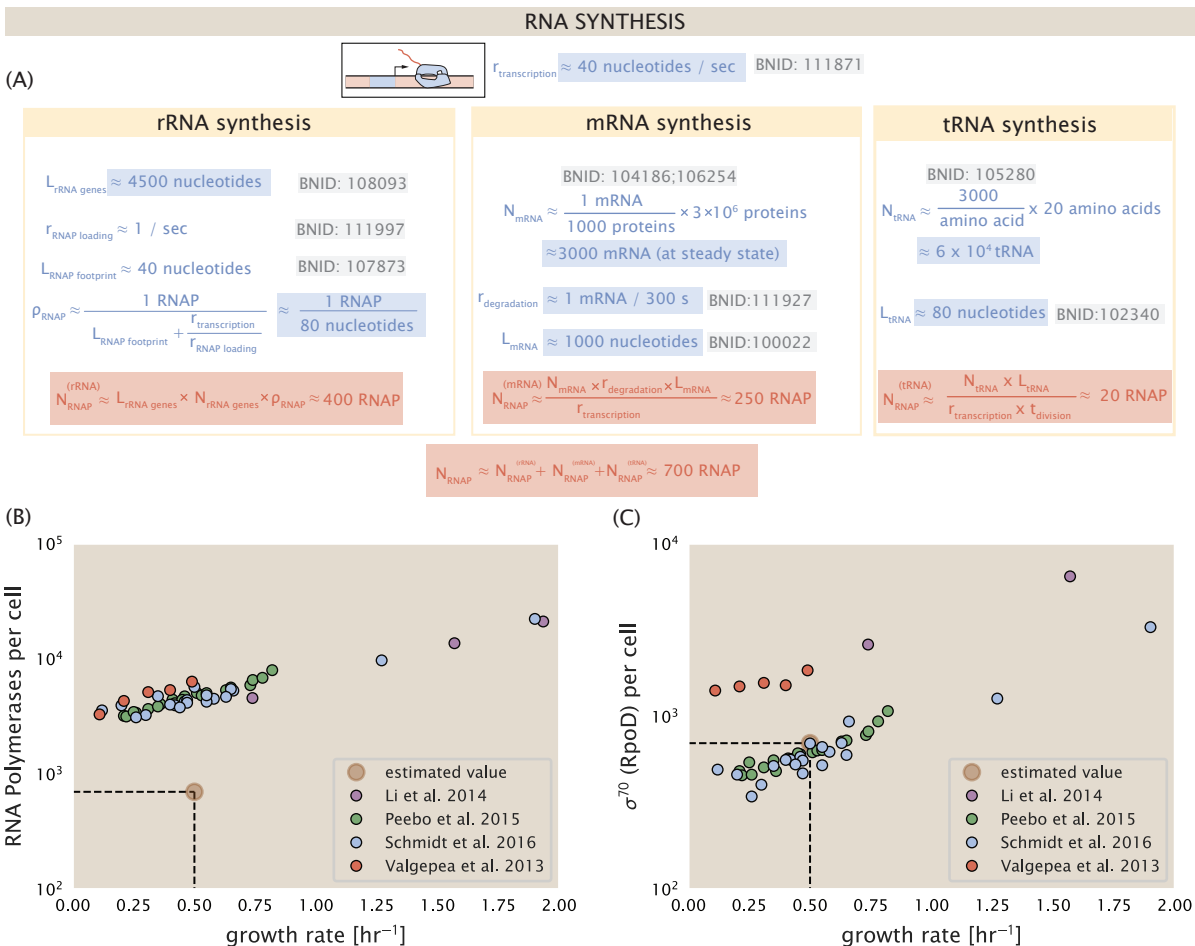


**Figure 5. Estimation of the RNA polymerase demand and comparison with experimental data.** (A) Estimations for the number of RNA polymerase needed to synthesize sufficient quantities of rRNA, mRNA, and tRNA from left to right, respectively. Bionumber Identifiers (BNIDs) are provided for key quantities used in the estimates. (B) The RNA polymerase core enzyme copy number as a function of growth rate. Colored points correspond to the average number RNA polymerase core enzymes that could be formed given a subunit stoichiometry of  $[RpoA]_2[RpoC][RpoB]$ . (C) The abundance of  $\sigma^{70}$  as a function of growth rate. Estimated value for the number of RNAP is shown in (B) and (C) as a translucent brown point at a growth rate of  $0.5 \text{ hr}^{-1}$ .

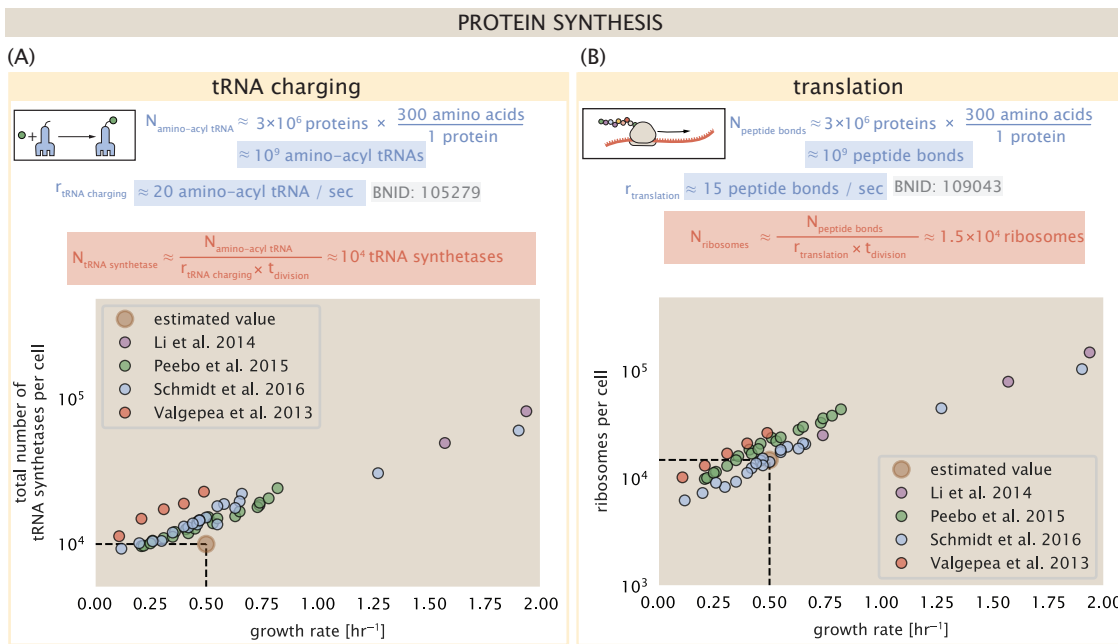


**Figure 6. Estimation of the required tRNA synthetases and ribosomes.** (A) Estimation for the number of tRNA synthetases that will supply the required amino acid demand. The sum of all tRNA synthetases copy numbers are plotted as a function of growth rate ([ArgS], [CysS], [GlnS], [GlxS], [IleS], [LeuS], [ValS], [AlaS]<sub>2</sub>, [AsnS]<sub>2</sub>, [AspS]<sub>2</sub>, [TyrS]<sub>2</sub>, [TrpS]<sub>2</sub>, [ThrS]<sub>2</sub>, [SerS]<sub>2</sub>, [ProS]<sub>2</sub>, [PheS]<sub>2</sub>[PheT]<sub>2</sub>, [MetG]<sub>2</sub>, [lysS]<sub>2</sub>, [HisS]<sub>2</sub>, [GlyS]<sub>2</sub>[GlyQ]<sub>2</sub>). (B) Estimation for the number of ribosomes required to synthesize all proteins in the cell. The average abundance of ribosomes is plotted as a function of growth rate. Our estimated values are shown for a growth rate of 0.5 hr<sup>-1</sup>.

384 While these estimates and comparison with experimental data reveal an interesting dynamic at  
 385 play between the transcriptional demand and copy numbers of the corresponding machinery, these  
 386 findings illustrate that transcription cannot be the rate limiting step in bacterial division. **Figure 5**  
 387 (A) reveals that the availability of RNA polymerase is not a limiting factor for cell division as the cell  
 388 always has an apparent ~10-fold excess than needed. Furthermore, if more transcriptional activity  
 389 was needed to satisfy the cellular requirements, more  $\sigma^{70}$ -factors could be expressed to utilize a  
 390 larger fraction of the RNA polymerase pool.

### 391 Protein synthesis

392 Lastly, we turn our attention to the process of translation. So far in our estimates there has been  
 393 little to suggest any apparent limit on the cell's ability to produce the required number protein  
 394 species. Even in our example of *E. coli* grown under different carbohydrate sources (**Figure 2(B)**), cells  
 395 are able to utilize alternative carbon sources by inducing the expression of additional membrane  
 396 transporters and enzymes. For a doubling time of 5000 seconds, *E. coli* has roughly  $3 \times 10^6$  proteins  
 397 per cell, which for an average protein of 300 aa, amounts to  $\approx 10^9$  peptide bonds that must be  
 398 formed. This also corresponds to the number of amino-acyl tRNA that are used, with the pool of  
 399 tRNA continuously recharged with new amino acids by tRNA synthetases. At a rate of charging of  
 400 about 20 amino-acyl tRNA per second (BNID: 105279, **Milo et al. (2010)**), we find that cells have more  
 401 than sufficient tRNA synthetases to provide the required amino-acyl tRNA that are then consumed  
 402 by ribosomes **Figure 6(A)**.

403 If we consider a translation elongation rate of  $\approx 15$  peptide bonds per second (BNID: 114271,  
 404 **Milo et al. (2010); Dai et al. (2016)**) cell needs  $1.5 \times 10^4$  ribosomes per cell at a growth rate of  $0.5 \text{ hr}^{-1}$ .  
 405 This is indeed consistent with the experimental data shown in **Figure 6(B)**. From the perspective of  
 406 asking whether the process of translation might be rate-limiting, it is useful to note that the core  
 407 ribosomal proteins take up as much as [] percent of proteome at the fastest growth rates we have  
 408 data on. This is in addition to other ribosomal proteins like the translation elongation factor EF-Tu

409 that is among the most highly expressed protein. One additional observation we made earlier in  
 410 our estimation of rRNA, was that the rRNA operons need to be nearly packed with transcribing RNA  
 411 polymerase in order to provide the required rRNA for each ribosome even at the slower growth rate  
 412 considered in our earlier estimate. Experimentally, consecutive deletion of rRNA operons showed a  
 413 significant reduction in growth rate in rich media when cells had only 3 or less (*Levin et al., 2017*).  
 414 Separately, it has been found that gross overexpression of a protein can dramatically lower growth  
 415 rate due to the altered allocation of resources (*Basan et al., 2015*). Optimal resource allocation and  
 416 how it relates to cell growth has been an area of intense quantitative study over the last decade by  
 417 Hwa and others (*Scott et al., 2010; Hui et al., 2015*).

418 We can begin to gain some intuition into how translation, or ribosomes more specifically, might  
 419 limit growth by noting that the total number of peptide bonds generated as the cell doubles,  $N_{aa}$ ,  
 420 will be given by,  $\tau \cdot r_t \cdot R$ . Here,  $\tau$  refers to the doubling time of the cell under steady-state growth,  $r_t$   
 421 is the maximum translation rate, and  $R$  is the average number of ribosomes in the cell. With the  
 422 growth rate related to the cell doubling time by  $\lambda = \ln(2)/\tau$ , we can write the translation-limited  
 423 growth rate as,

$$\lambda_{\text{translation-limited}} = \frac{\ln(2) \cdot r_t \cdot R}{N_{aa}}. \quad (1)$$

424 Alternatively, since  $N_{aa}$  is related to the total protein mass through the molecular weight of each  
 425 protein, we can also consider the growth rate in terms of ribosomal mass fraction. An approximation,  
 426 assuming an average amino acid molecular weight of 110 Da is shown in **Figure 7(A)**. This allows us  
 427 to rewrite the growth rate as,

$$\lambda_{\text{translation-limited}} \approx \frac{\ln(2) \cdot r_t}{L_R} \Phi_R, \quad (2)$$

428 where  $L_R$  is the total length in amino acids that make up a ribosome, and  $\Phi_R$  is the ribosomal mass  
 429 fraction. This is plotted as a function of ribosomal fraction  $\Phi_R$  in **Figure 7(A)**, where  $L_R \approx 8,000$  aa,  
 430 corresponds to the length in amino acids for all ribosomal subunits of the 50S and 30S complexes  
 431 and EF-Tu.

432 Perhaps the first thing to notice is that there is a maximum growth rate at about  $\lambda \approx 6\text{hr}^{-1}$ , or  
 433 doubling time of about 7 minutes (dashed line). This growth rate can be viewed as an inherent  
 434 maximum rate due to the need for the cell to double the cell's entire ribosomal mass. Interestingly,  
 435 this limit is independent of the absolute number of ribosomes, but rather is simply given by  
 436 time to translate an entire ribosome,  $L_R/r_t$ . As shown in **Figure 7(B)**, we can reconcile this with  
 437 the observation that in order to double the average number of ribosomes, each ribosome must  
 438 produce a second ribosome. This is a process that cannot be parallelized.

439 For reasonable values of  $\Phi_R$ , in the range of about 0.1 - 0.3 (*Scott et al., 2010*), the maximum  
 440 growth rate is in line with experimentally reported growth rates around 0.5 - 2  $\text{hr}^{-1}$ . Here we have  
 441 implicitly assumed that translation proceeds randomly, without preference between ribosomal or  
 442 non-ribosomal mRNA, which appears reasonable. Importantly, in order for a cell to scale this limit  
 443 set by  $\Phi_R$  the cell must increase its ribosomal abundance, either by synthesizing more ribosomes  
 444 or reducing the fraction of non-ribosomal proteins.

445 One last point to note is that across different species of bacteria, while it is common for bacteria  
 446 to decrease their ribosomal abundance in poorer nutrient conditions, this does not decrease to  
 447 zero (*Scott et al. (2010); Liebermeister et al. (2014)*). From the perspective of a bacterium dealing  
 448 with uncertain nutrient conditions, there is likely a benefit for the cell to maintain some relative  
 449 fraction of ribosomes to support rapid growth as nutrient conditions improve. If we consider a  
 450 scenario where nutrient conditions become poorer and poorer, there must be a regime where the  
 451 cell has more ribosomes than it can utilize. In order for a cell to maintain steady-state growth, it will  
 452 need to attenuate its translational activity since ribosomes would otherwise exhaust their supply of  
 453 amino acids and bring cell growth to a halt (**Figure 7(C)**). We will consider this more specifically for *E. coli*  
 454 in the next section by considering recent experimental work.

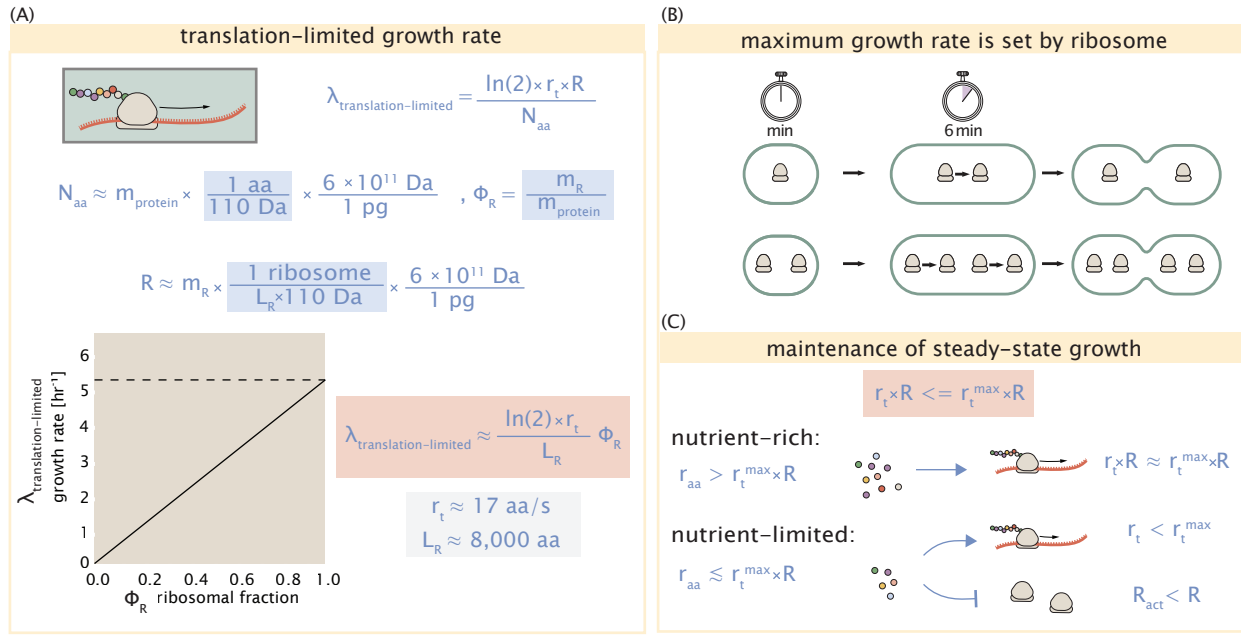


**Figure 7. Translation-limited growth rate.** (A) Here we consider the translation-limited growth as a function of ribosomal fraction. By mass balance, the time required to double the entire proteome ( $N_{\text{aa}} / r_t$ ) sets the translation-limited growth rate,  $\lambda_{\text{translation-limited}}$ . Here  $N_{\text{aa}}$  is effectively the number of peptide bonds that must be translated,  $r_t$  is the translation elongation rate, and  $R$  is the number of ribosomes. This can also be re-written in terms of the ribosomal mass fraction  $\Phi_R = m_R / m_{\text{protein}}$ , where  $m_R$  is the total ribosomal mass and  $m_{\text{protein}}$  is the mass of all proteins in the cell.  $L_R$  refers to the summed length of the ribosome in amino acids.  $\lambda_{\text{translation-limited}}$  is plotted as a function of  $\Phi_R$  (solid line). (B) The dashed line in part (A) identifies a maximum growth rate that is set by the ribosome. Specifically, this growth rate corresponds to the time required to translate an entire ribosome,  $L_R / r_t$ . This is a result that is independent of the number of ribosomes in the cell as shown schematically here. (C) Schematic showing

455 **Multiple replication forks provide a strategy to bias ribosome abundance.**

456 One feature of *E. coli*, as well as other bacteria like *B. subtilis*, is their growth by an adder type  
 457 mechanism whereby cells add a constant volume with each cell division (*Taheri-Araghi et al., 2015*).  
 458 In conjunction with this, additional rounds of DNA replication are triggered when cells reach a critical  
 459 volume per origin of replication (*Figure 8(A)*). This leads to the classically-described exponential  
 460 increase in cell size with growth rate *Schaechter et al. (1958); Si et al. (2017, 2019)*. In the context of  
 461 maximizing growth rate, it is notable that the majority of ribosomal proteins and rRNA operons are  
 462 found closer to the DNA origin, with an increase in rRNA gene dosage needed in order to meet the  
 463 demand of an increasingly larger cell at faster growth. This raises the possibility that the observed  
 464 global proteome allocation and specifically, the increased synthesis of ribosomes may be in part a  
 465 consequence of increased gene dosage for genes near the DNA origin.

466 While a bias in gene dosage and transcription is observed for genes near the origin for rapidly  
 467 growing *E. coli* (*Scholz et al., 2019*), we are unaware of such characterization at the proteomic level.  
 468 In order to do so with our data, we calculated a running boxcar average of protein copy number as  
 469 a function of the transcriptional start site associated with each protein. While absolute protein copy  
 470 numbers vary substantially across the chromosome, we indeed observe a skew in average protein  
 471 abundance for genes under the fastest growth conditions (*Figure 8(B)*, showing the result using a  
 472 0.5 kb averaging window). The large positive increases in copy number near the DNA origin largely  
 473 reflect an increase in absolute abundance of ribosomal proteins. This is in contrast to slower growth  
 474 conditions where the average copy number is more uniform across the length of the chromosome.

475 If ribosomal genes (rRNA and ribosomal proteins) are being synthesized according to their  
 476 available gene dosage we can make two related hypotheses about how ribosomal abundance  
 477 should vary with DNA content. The first is that the ribosomal protein fraction should increase  
 478 in proportion to the average ratio of DNA origins to DNA termini ( $\langle \text{ori} \rangle / \langle \text{ter} \rangle$  ratio), which is a  
 479 consequence of the skew in DNA dosage as cells grow faster than we considered in *Figure 8(B)*. The  
 480 second is that the absolute number of ribosomes should increase in proportion to the number of  
 481 DNA origins ( $\langle \text{ori} \rangle$ ), since this will reflect the total gene dosage in the cell at a particular growth  
 482 condition.

483 In order to test these hypotheses we consider the experimental data from *Si et al.* ( $\langle \text{ori} \rangle / \langle \text{ter} \rangle$   
 484 ratio) depends on how quickly chromosomes ( $\tau_C$ , referring to the C period of cell division) are repli-  
 485 cated relative the cell's doubling time  $\tau$  and is given by  $2^{\tau_C/\tau} = 2^{\tau_C \cdot \ln(2)/\lambda}$ . In *translation\_e.coli(C)* we plot  $\tau_C$   
 486 versus  $\tau$  that were measured, with data points in red corresponding to *E. coli* strain MG1655, and  
 487 blue to strain NCM3722. In their work they also measured the total RNA to protein ratio which  
 488 reflects ribosomal abundance and we show that data along with other recent measurements from  
 489 *Dai et al.*. Indeed there appears to be a strong correlation between ribosomal abundance and the  
 490 estimated  $\langle \text{ori} \rangle / \langle \text{ter} \rangle$ . [NB: should I calculate a correlation coefficient?]. We can similarly estimate  
 491  $\langle \text{ori} \rangle$ , which depends on how often replication forks are initiated per cell cycle. This is given by the  
 492 number of overlapping cell cycles,  $2^{\tau_{\text{cyc}}/\tau} = 2^{\tau_{\text{cyc}} \cdot \ln(2)/\lambda}$ , where  $\tau_{\text{cyc}}$ , where  $\tau_{\text{cyc}}$  refers to the total time of  
 493 chromosome replication and cell division. The top plot in *Figure 8(D)* shows the associated data  
 494 from *Si et al.*, which we use to estimate  $\langle \text{ori} \rangle$  for each growth condition of the proteomic data. In  
 495 agreement with our expectations, we find a strong correlation between the ribosome copy number  
 496 and estimated  $\langle \text{ori} \rangle$ .

497 **References**

- 498 Abelson, H., Johnson, L., Penman, S., and Green, H. (1974). Changes in RNA in relation to growth of the fibroblast:  
 499 II. The lifetime of mRNA, rRNA, and tRNA in resting and growing cells. *Cell*, 1(4):161–165.
- 500 Aidelberg, G., Towbin, B. D., Rothschild, D., Dekel, E., Bren, A., and Alon, U. (2014). Hierarchy of non-glucose  
 501 sugars in *Escherichia coli*. *BMC Systems Biology*, 8(1):133.
- 502 Antonenko, Y. N., Pohl, P., and Denisov, G. A. (1997). Permeation of ammonia across bilayer lipid membranes  
 503 studied by ammonium ion selective microelectrodes. *Biophysical Journal*, 72(5):2187–2195.

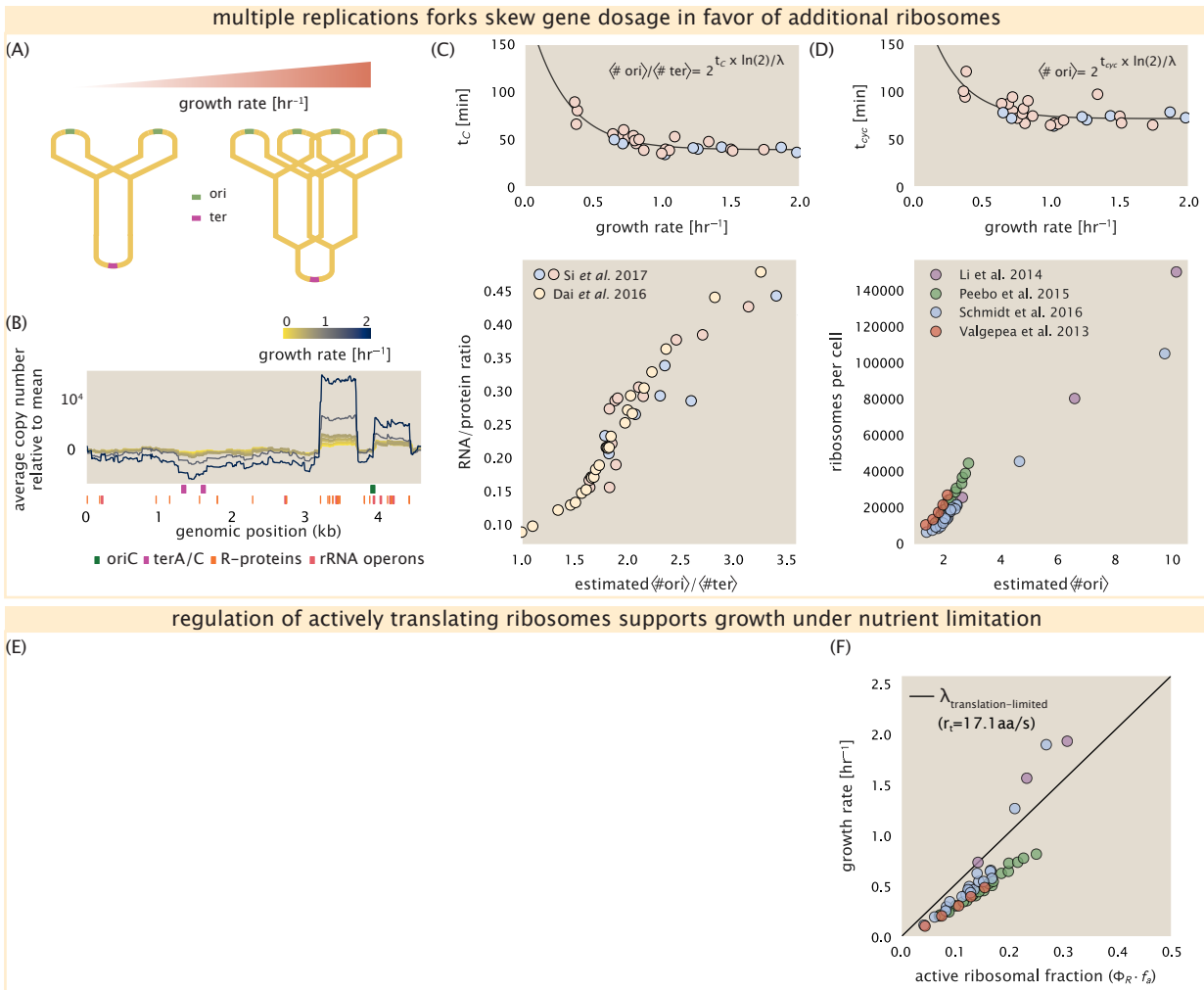


**Figure 8. Multiple replication forks skew gene dosage and ribosomal content.** (A) Schematic shows the expected increase in replication forks (or number of ori regions) as *E. coli* cells grow faster. (B) The average copy number is calculated at each position along the chromosome by running boxcar average with a 0.5 kb averaging window. Top plots in (C) and (D) show experimental data from Si *et al.* (2017) Solid lines show fits to the data, which were used to estimate  $\langle \text{ori} \rangle / \langle \text{ter} \rangle$  and  $\langle \# \text{ori} \rangle$  [NB: to note fit equations]. Red data points correspond to measurements in strain MG1655, while blue points are for strain NCM3722. Bottom plot in (C) compares our estimate of  $\langle \text{ori} \rangle / \langle \text{ter} \rangle$  to the experimental measurements of ribosomal abundance via RNA/protein ratios. Yellow data points correspond to measurements from Dai *et al.* (2016), while the red and blue data points come from Si *et al.* (2017). The bottom plot in (D) plots the ribosome copy number from the proteomic data against our estimate of  $\langle \# \text{ori} \rangle$ . (E) [in progress], (F) Experimental data from Dai *et al.* are used to estimate the fraction of actively translating ribosomes. The solid line represents the translation-limited growth rate for ribosomes elongating at 17.1 aa/s.

- 504 Ason, B., Bertram, J. G., Hingorani, M. M., Beechem, J. M., O'Donnell, M., Goodman, M. F., and Bloom, L. B.  
 505 (2000). A Model for *Escherichia coli* DNA Polymerase III Holoenzyme Assembly at Primer/Template Ends:  
 506 DNA Triggers A Change In Binding Specificity of the  $\gamma$  Complex Clamp Loader. *Journal of Biological Chemistry*,  
 507 275(4):3006–3015.
- 508 Assentoft, M., Kaptan, S., Schneider, H.-P., Deitmer, J. W., de Groot, B. L., and MacAulay, N. (2016). Aquaporin 4  
 509 as a NH<sub>3</sub> Channel. *Journal of Biological Chemistry*, 291(36):19184–19195.
- 510 Basan, M., Zhu, M., Dai, X., Warren, M., Sévin, D., Wang, Y.-P., and Hwa, T. (2015). Inflating bacterial cells by  
 511 increased protein synthesis. *Molecular Systems Biology*, 11(10):836.
- 512 Bauer, S. and Ziv, E. (1976). Dense growth of aerobic bacteria in a bench-scale fermentor. *Biotechnology and*  
 513 *Bioengineering*, 18(1):81–94. \_eprint: <https://onlinelibrary.wiley.com/doi/10.1002/bit.260180107>.
- 514 Belliveau, N. M., Barnes, S. L., Ireland, W. T., Jones, D. L., Sweredoski, M. J., Moradian, A., Hess, S., Kinney, J. B., and  
 515 Phillips, R. (2018). Systematic approach for dissecting the molecular mechanisms of transcriptional regulation  
 516 in bacteria. *Proceedings of the National Academy of Sciences*, 115(21):E4796–E4805.
- 517 Birnbaum, L. S. and Kaplan, S. (1971). Localization of a Portion of the Ribosomal RNA Genes in *Escherichia coli*.  
 518 *Proceedings of the National Academy of Sciences*, 68(5):925–929.
- 519 Booth, I. R., Mitchell, W. J., and Hamilton, W. A. (1979). Quantitative analysis of proton-linked transport systems.  
 520 The lactose permease of *Escherichia coli*. *Biochemical Journal*, 182(3):687–696.
- 521 Bremer, H. and Dennis, P. P. (2008). Modulation of Chemical Composition and Other Parameters of the Cell at  
 522 Different Exponential Growth Rates. *EcoSal Plus*, 3(1).
- 523 Browning, D. F. and Busby, S. J. W. (2016). Local and global regulation of transcription initiation in bacteria.  
 524 *Nature Reviews Microbiology*, 14(10):638–650.
- 525 Dai, X., Zhu, M., Warren, M., Balakrishnan, R., Patsalo, V., Okano, H., Williamson, J. R., Fredrick, K., Wang, Y.-P.,  
 526 and Hwa, T. (2016). Reduction of translating ribosomes enables *Escherichia coli* to maintain elongation rates  
 527 during slow growth. *Nature Microbiology*, 2(2):16231.
- 528 Escalante, A., Salinas Cervantes, A., Gosset, G., and Bolívar, F. (2012). Current knowledge of the *Escherichia coli*  
 529 phosphoenolpyruvate-carbohydrate phosphotransferase system: Peculiarities of regulation and impact on  
 530 growth and product formation. *Applied Microbiology and Biotechnology*, 94(6):1483–1494.
- 531 Feist, A. M., Henry, C. S., Reed, J. L., Krummenacker, M., Joyce, A. R., Karp, P. D., Broadbelt, L. J., Hatzimanikatis, V.,  
 532 and Palsson, B. Ø. (2007). A genome-scale metabolic reconstruction for *Escherichia coli* K-12 MG1655 that  
 533 accounts for 1260 ORFs and thermodynamic information. *Molecular Systems Biology*, 3(1):121.
- 534 Fijalkowska, I. J., Schaaper, R. M., and Jonczyk, P. (2012). DNA replication fidelity in *Escherichia coli*: A multi-DNA  
 535 polymerase affair. *FEMS Microbiology Reviews*, 36(6):1105–1121.
- 536 Finkelstein, I. J. and Greene, E. C. (2013). Molecular Traffic Jams on DNA. *Annual Review of Biophysics*, 42(1):241–  
 537 263.
- 538 Gama-Castro, S., Salgado, H., Santos-Zavaleta, A., Ledezma-Tejeida, D., Muñiz-Rascado, L., García-Sotelo, J. S.,  
 539 Alquicira-Hernández, K., Martínez-Flores, I., Pannier, L., Castro-Mondragón, J. A., Medina-Rivera, A., Solano-Lira,  
 540 H., Bonavides-Martínez, C., Pérez-Rueda, E., Alquicira-Hernández, S., Porron-Sotelo, L., López-Fuentes, A.,  
 541 Hernández-Koutoucheva, A., Moral-Chávez, V. D., Rinaldi, F., and Collado-Vides, J. (2016). RegulonDB version  
 542 9.0: High-level integration of gene regulation, coexpression, motif clustering and beyond. *Nucleic Acids  
 543 Research*, 44(D1):D133–D143.
- 544 Ge, J., Yu, G., Ator, M. A., and Stubbe, J. (2003). Pre-Steady-State and Steady-State Kinetic Analysis of *E. coli* Class I  
 545 Ribonucleotide Reductase. *Biochemistry*, 42(34):10071–10083.
- 546 Goldman, S. R., Nair, N. U., Wells, C. D., Nickels, B. E., and Hochschild, A. (2015). The primary  $\sigma$  factor in *Escherichia*  
 547 *coli* can access the transcription elongation complex from solution *in vivo*. *eLife*, 4:e10514.
- 548 Harris, R. M., Webb, D. C., Howitt, S. M., and Cox, G. B. (2001). Characterization of PitA and PitB from *Escherichia*  
 549 *coli*. *Journal of Bacteriology*, 183(17):5008–5014.
- 550 Heldal, M., Norland, S., and Tumyr, O. (1985). X-ray microanalytic method for measurement of dry matter and  
 551 elemental content of individual bacteria. *Applied and Environmental Microbiology*, 50(5):1251–1257.

- 552 Hui, S., Silverman, J. M., Chen, S. S., Erickson, D. W., Basan, M., Wang, J., Hwa, T., and Williamson, J. R. (2015).  
 553 Quantitative proteomic analysis reveals a simple strategy of global resource allocation in bacteria. *Molecular Systems Biology*, 11(2):e784–e784.
- 555 Ireland, W. T., Beeler, S. M., Flores-Bautista, E., Belliveau, N. M., Sweredoski, M. J., Moradian, A., Kinney, J. B., and  
 556 Phillips, R. (2020). Deciphering the regulatory genome of *Escherichia coli*, one hundred promoters at a time. *bioRxiv*.
- 558 Jacob, F. and Monod, J. (1961). Genetic regulatory mechanisms in the synthesis of proteins. *Journal of Molecular Biology*, 3(3):318–356.
- 560 Jensen, R. B., Wang, S. C., and Shapiro, L. (2001). A moving DNA replication factory in *Caulobacter crescentus*.  
 561 *The EMBO journal*, 20(17):4952–4963.
- 562 Jun, S., Si, F., Pugatch, R., and Scott, M. (2018). Fundamental principles in bacterial physiology - history, recent  
 563 progress, and the future with focus on cell size control: A review. *Reports on Progress in Physics*, 81(5):056601.
- 564 Kapanidis, A. N., Margeat, E., Laurence, T. A., Doose, S., Ho, S. O., Mukhopadhyay, J., Kortkhonjia, E., Mekler, V.,  
 565 Ebright, R. H., and Weiss, S. (2005). Retention of Transcription Initiation Factor  $\Sigma$ 70 in Transcription Elongation:  
 566 Single-Molecule Analysis. *Molecular Cell*, 20(3):347–356.
- 567 Khademi, S., O'Connell, J., Remis, J., Robles-Colmenares, Y., Miercke, L. J. W., and Stroud, R. M. (2004). Mechanism  
 568 of Ammonia Transport by Amt/MEP/Rh: Structure of AmtB at 1.35 Å. *Science*, 305(5690):1587–1594.
- 569 Levin, B. R., McCall, I. C., Perrot, V., Weiss, H., Ovesepian, A., and Baquero, F. (2017). A Numbers Game: Ribosome  
 570 Densities, Bacterial Growth, and Antibiotic-Mediated Stasis and Death. *mBio*, 8(1).
- 571 Li, G.-W., Burkhardt, D., Gross, C., and Weissman, J. S. (2014). Quantifying absolute protein synthesis rates  
 572 reveals principles underlying allocation of cellular resources. *Cell*, 157(3):624–635.
- 573 Liebermeister, W., Noor, E., Flamholz, A., Davidi, D., Bernhardt, J., and Milo, R. (2014). Visual account of protein  
 574 investment in cellular functions. *Proceedings of the National Academy of Sciences*, 111(23):8488–8493.
- 575 Liu, M., Durfee, T., Cabrera, J. E., Zhao, K., Jin, D. J., and Blattner, F. R. (2005). Global Transcriptional Programs  
 576 Reveal a Carbon Source Foraging Strategy by *Escherichia coli*. *Journal of Biological Chemistry*, 280(16):15921–  
 577 15927.
- 578 Milo, R., Jorgensen, P., Moran, U., Weber, G., and Springer, M. (2010). BioNumbers—the database of key numbers  
 579 in molecular and cell biology. *Nucleic Acids Research*, 38(suppl\_1):D750–D753.
- 580 Monod, J. (1947). The phenomenon of enzymatic adaptation and its bearings on problems of genetics and  
 581 cellular differentiation. *Growth Symposium*, 9:223–289.
- 582 Mooney, R. A., Darst, S. A., and Landick, R. (2005). Sigma and RNA Polymerase: An On-Again, Off-Again  
 583 Relationship? *Molecular Cell*, 20(3):335–345.
- 584 Mooney, R. A. and Landick, R. (2003). Tethering  $\Sigma$ 70 to RNA polymerase reveals high in vivo activity of  $\sigma$  factors  
 585 and  $\Sigma$ 70-dependent pausing at promoter-distal locations. *Genes & Development*, 17(22):2839–2851.
- 586 Neidhardt, F. C., Ingraham, J., and Schaechter, M. (1991). *Physiology of the Bacterial Cell - A Molecular Approach*,  
 587 volume 1. Elsevier.
- 588 Patrick, M., Dennis, P. P., Ehrenberg, M., and Bremer, H. (2015). Free RNA polymerase in *Escherichia coli*. *Biochimie*,  
 589 119:80–91.
- 590 Peebo, K., Valgepea, K., Maser, A., Nahku, R., Adamberg, K., and Vilu, R. (2015). Proteome reallocation in  
 591 *Escherichia coli* with increasing specific growth rate. *Molecular BioSystems*, 11(4):1184–1193.
- 592 Perdue, S. A. and Roberts, J. W. (2011).  $\sigma^{70}$ -dependent Transcription Pausing in *Escherichia coli*. *Journal of  
 593 Molecular Biology*, 412(5):782–792.
- 594 Phillips, R. (2018). Membranes by the Numbers. In *Physics of Biological Membranes*, pages 73–105. Springer,  
 595 Cham, Cham.
- 596 Ramos, S. and Kaback, H. R. (1977). The relation between the electrochemical proton gradient and active  
 597 transport in *Escherichia coli* membrane vesicles. *Biochemistry*, 16(5):854–859.

- 598 Rosenberg, H., Gerdes, R. G., and Chegwidden, K. (1977). Two systems for the uptake of phosphate in *Escherichia*  
599 *coli*. *Journal of Bacteriology*, 131(2):505–511.
- 600 Rudd, S. G., Valerie, N. C. K., and Helleday, T. (2016). Pathways controlling dNTP pools to maintain genome  
601 stability. *DNA Repair*, 44:193–204.
- 602 Sánchez-Romero, M. A., Molina, F., and Jiménez-Sánchez, A. (2011). Organization of ribonucleoside diphosphate  
603 reductase during multifork chromosome replication in *Escherichia coli*. *Microbiology*, 157(8):2220–2225.
- 604 Schaechter, M., Maaløe, O., and Kjeldgaard, N. O. (1958). Dependency on Medium and Temperature of Cell Size  
605 and Chemical Composition during Balanced Growth of *Salmonella typhimurium*. *Microbiology*, 19(3):592–606.
- 606 Schmidt, A., Kochanowski, K., Vedelaar, S., Ahrné, E., Volkmer, B., Callipo, L., Knoops, K., Bauer, M., Aebersold,  
607 R., and Heinemann, M. (2016). The quantitative and condition-dependent *Escherichia coli* proteome. *Nature  
Biotechnology*, 34(1):104–110.
- 608 Scholz, S. A., Diao, R., Wolfe, M. B., Fivenson, E. M., Lin, X. N., and Freddolino, P. L. (2019). High-Resolution  
609 Mapping of the *Escherichia coli* Chromosome Reveals Positions of High and Low Transcription. *Cell Systems*,  
610 8(3):212–225.e9.
- 611 Scott, M., Gunderson, C. W., Mateescu, E. M., Zhang, Z., and Hwa, T. (2010). Interdependence of cell growth and  
612 gene expression: origins and consequences. *Science*, 330(6007):1099–1102.
- 613 Sekowska, A., Kung, H.-F., and Danchin, A. (2000). Sulfur Metabolism in *Escherichia coli* and Related Bacteria:  
614 Facts and Fiction. *Journal of Molecular Microbiology and Biotechnology*, 2(2):34.
- 615 Si, F., Le Treut, G., Sauls, J. T., Vadia, S., Levin, P. A., and Jun, S. (2019). Mechanistic Origin of Cell-Size Control and  
616 Homeostasis in Bacteria. *Current Biology*, 29(11):1760–1770.e7.
- 617 Si, F., Li, D., Cox, S. E., Sauls, J. T., Azizi, O., Sou, C., Schwartz, A. B., Erickstad, M. J., Jun, Y., Li, X., and Jun, S. (2017).  
618 Invariance of Initiation Mass and Predictability of Cell Size in *Escherichia coli*. *Current Biology*, 27(9):1278–1287.
- 619 Sirko, A., Zatyka, M., Sadowsy, E., and Hulanicka, D. (1995). Sulfate and thiosulfate transport in *Escherichia coli*  
620 K-12: Evidence for a functional overlapping of sulfate- and thiosulfate-binding proteins. *Journal of Bacteriology*,  
621 177(14):4134–4136.
- 622 Stasi, R., Neves, H. I., and Spira, B. (2019). Phosphate uptake by the phosphonate transport system PhnCDE.  
623 *BMC Microbiology*, 19.
- 624 Stevenson, B. S. and Schmidt, T. M. (2004). Life History Implications of rRNA Gene Copy Number in *Escherichia  
625 coli*. *Applied and Environmental Microbiology*, 70(11):6670–6677.
- 626 Svenningsen, S. L., Kongstad, M., Stenum, T. S. n., Muñoz-Gómez, A. J., and Sørensen, M. A. (2017). Transfer RNA  
627 is highly unstable during early amino acid starvation in *Escherichia coli*. *Nucleic Acids Research*, 45(2):793–804.
- 628 Szenk, M., Dill, K. A., and de Graff, A. M. R. (2017). Why Do Fast-Growing Bacteria Enter Overflow Metabolism?  
629 Testing the Membrane Real Estate Hypothesis. *Cell Systems*, 5(2):95–104.
- 630 Taheri-Araghi, S., Bradde, S., Sauls, J. T., Hill, N. S., Levin, P. A., Paulsson, J., Vergassola, M., and Jun, S. (2015).  
631 Cell-size control and homeostasis in bacteria. - PubMed - NCBI. *Current Biology*, 25(3):385–391.
- 632 Taymaz-Nikerel, H., Borujeni, A. E., Verheijen, P. J. T., Heijnen, J. J., and van Gulik, W. M.  
633 (2010). Genome-derived minimal metabolic models for *Escherichia coli* MG1655 with estimated  
634 in vivo respiratory ATP stoichiometry. *Biotechnology and Bioengineering*, 107(2):369–381. \_eprint:  
635 https://onlinelibrary.wiley.com/doi/pdf/10.1002/bit.22802.
- 636 Valgepea, K., Adamberg, K., Seiman, A., and Vilu, R. (2013). *Escherichia coli* achieves faster growth by increasing  
637 catalytic and translation rates of proteins. *Molecular BioSystems*, 9(9):2344.
- 638 van Heeswijk, W. C., Westerhoff, H. V., and Boogerd, F. C. (2013). Nitrogen Assimilation in *Escherichia coli*: Putting  
639 Molecular Data into a Systems Perspective. *Microbiology and Molecular Biology Reviews*, 77(4):628–695.
- 640 Willsky, G. R., Bennett, R. L., and Malamy, M. H. (1973). Inorganic Phosphate Transport in *Escherichia coli*:  
641 Involvement of Two Genes Which Play a Role in Alkaline Phosphatase Regulation. *Journal of Bacteriology*,  
642 113(2):529–539.

- 644 Zhang, L., Jiang, W., Nan, J., Almqvist, J., and Huang, Y. (2014a). The *Escherichia coli* CysZ is a pH dependent  
645 sulfate transporter that can be inhibited by sulfite. *Biochimica et Biophysica Acta (BBA) - Biomembranes*,  
646 1838(7):1809–1816.
- 647 Zhang, Z., Aboulwafa, M., and Saier, M. H. (2014b). Regulation of crp gene expression by the catabolite  
648 repressor/activator, cra, in *Escherichia coli*. *Journal of Molecular Microbiology and Biotechnology*, 24(3):135–141.